Materials Science Forum
ISSN: 1662-9752, Vol. 1187, pp 45-54
doi:10.4028/p-GJcp8x

Submitted: 2025-12-19
Revised: 2026-02-20
Accepted: 2026-02-20
Online: 2026-04-17

Shape Memory Behavior of 3D-Printed Biomedical Polyurethane with Room Temperature Transition

Denise BELLISARIO[1,a*], Leandro IORIO[2,b], Alice PROIETTI[1,c], Dounia NOQRA[1,d], Giorgio PATRIZII[1,e], Fabrizio QUADRINI[1,f] and Loredana SANTO[1,g]

[1]Department of Industrial Engineering, University of Rome Tor Vergata, via del Politecnico 1, Rome, Italy

[2]Department of Engineering and Science, Mercatorum University, p.zza Mattei 10, Rome, Italy

[a]denise.bellisario@uniroma2.it, [b]leandro.iorio@unimercatorum.it, [c]alice.proietti@uniroma2.it, [d]dounia.noqra@uniroma2.it, [e]giorgio.patrizii@uniroma2.it, [f]fabrizio.quadrini@uniroma2.it, [g]loredana.santo@uniroma2.it

Keywords: shape memory polymers, biomedical polyurethane, 3D printing.

Abstract. Shape memory polymers (SMPs) can recover from a programmed temporary shape to their original configuration when exposed to an external stimulus, most commonly heat, making them attractive materials for soft actuation in functional and biomedical devices. Among them, thermoplastic polyurethanes (TPUs) display reliable shape-memory behavior under various conditions. The emergence of biomedical-grade TPUs and their compatibility with additive manufacturing provides new opportunities for fabricating customized components with tunable actuation capabilities. In this study, biomedical TPU filaments were processed via fused deposition modeling (FDM) to produce block-shaped specimens of controlled size and weight. The samples were mechanically deformed into a C-shaped geometry at room temperature, fixed in fridge at the temperature of –20 °C, and subsequently tested under constrained recovery at room conditions, using a universal testing machine. The recovery load has been measured for a time of 30 min. The results show that TPU-based SMPs can develop substantial recovery forces during shape restoration. The shape memory behavior has been modeled by using a logistic function, which has been able to identify a characteristic time, the same for all the samples despite their printing conditions and architecture. These findings highlight the potential of FDM-processed biomedical TPUs for compact soft-actuation systems requiring high force output.

Introduction

In recent decades, advanced polymeric materials have attracted substantial interest in both academic research and industrial practice owing to their broad functional versatility, low density, and straightforward processability. Their properties can be precisely engineered through molecular design or by incorporating targeted additives and fillers, enabling the development of materials tailored for specific functional demands. Among these, shape-memory polymers (SMPs) stand out for their capacity to undergo large, recoverable deformations and to return to their programmed permanent shape upon exposure to an external stimulus. This unique behavior has facilitated their integration into a wide range of applications, including aerospace systems, biomedical devices, actuators, sensors, and smart textiles.

SMPs can be triggered by diverse stimuli such as heat, light, electric or magnetic fields, or humidity. After being deformed and fixed into a temporary configuration, they recover their initial shape once the appropriate stimulus is applied [1–4]. Their increasing relevance stems not only from their intrinsic functional performance but also from their compatibility with lightweight and sustainable design strategies, positioning them as strong candidates for next-generation smart materials and adaptive devices.

Among SMP families, thermoplastic polyurethanes (TPUs) have emerged as particularly versatile due to their segmented molecular architecture, which consists of alternating soft and hard domains.

This structure imparts high elasticity, tunable mechanical strength, thermal stability, and excellent resistance to abrasion and chemicals [5–9]. As a result, TPUs are widely used in biomedical engineering for implants and prosthetic components [10–12], in smart textiles for wearable electronics and responsive fabrics [13,14], and in adaptive or reconfigurable systems, including deployable structures and actuation mechanisms [15–17].

A rapidly expanding application area for SMPs—especially TPU-based systems—is soft robotics, a field focused on developing flexible, compliant, and adaptive robotic platforms inspired by biological organisms. In contrast to conventional robots composed of rigid, articulated elements, soft robots employ deformable materials such as elastomers and SMPs, enabling them to bend, stretch, and safely interact with humans and delicate environments [18,19]. The combination of processability, mechanical robustness, and stimulus-responsive behavior makes TPUs highly suitable for soft robotic components, including artificial muscles, gripping devices, and wearable interfaces, where efficient and reliable shape-memory actuation is essential. Parallel to these developments, additive manufacturing—particularly fused deposition modeling (FDM)—has become an attractive route for processing TPUs into complex geometries suitable for customized functional devices. Recent advances in additive manufacturing have further expanded the applicability of TPU-based SMPs. In particular, fused deposition modeling (FDM) has proven highly suitable for processing TPUs into complex geometries while maintaining their elastomeric and shape-memory characteristics [13–16]. Several studies have demonstrated that printing parameters—such as extrusion temperature, raster orientation, layer height, and cooling rate—strongly influence the microstructure, mechanical response, and thermal-triggered recovery behavior of FDM-printed TPU components [13,14]. Early work by Koehler et al. demonstrated that TPUs can be successfully processed by FDM while preserving their ability to undergo large recoverable deformations and reliable shape-memory cycling [20]. Since then, subsequent studies have shown that key printing parameters such as extrusion temperature, raster orientation, cooling rate, and infill architecture critically influence the microstructure and thermomechanical properties of printed TPU components. For example, Ritzen et al. confirmed that the FDM process alters the polymer's internal morphology, affecting stiffness, ductility, and long-term durability [21], while Rigotti et al. demonstrated that TPU blends printed via FDM can be functionalized to incorporate thermal energy storage or controlled release capabilities [22].

Several recent studies have focused specifically on the shape-memory performance of 3D-printed TPU-based systems. Rahmatabadi et al. investigated TPU-containing blends fabricated by FDM and showed that printing conditions strongly affect shape fixity, recovery stress, and recovery ratio, highlighting the importance of process optimization when designing SMP actuators [23]. Similarly, Peng et al. reported that TPU-based polymer blends produced via 4D printing can exhibit high extensibility, efficient shape recovery, and even self-healing behavior, underscoring the potential of printed TPUs for multifunctional soft actuators [24]. Investigations by Jung and Jung further demonstrated that FDM-printed TPU structures with engineered geometries can achieve programmable shape-change pathways, enabling advanced compliance and deformation control for soft robotic components [25].

Beyond experimental characterization, predictive modeling of shape-memory polymer (SMP) behavior plays a fundamental role in understanding and designing shape-memory-based actuation systems. Over the past two decades, a wide range of modeling approaches has been proposed to describe the thermomechanical response of SMPs, including micromechanical formulations, phase-transition-based theories, and phenomenological viscoelastic frameworks [26–28]. Many constitutive models relate shape recovery to temperature-dependent phase evolution between soft and hard domains or to time-dependent molecular relaxation mechanisms governing stress release and strain recovery during activation [29,30].

In practical applications as in soft actuators or biomedical devices, the time-dependent evolution of shape recovery is often critical as well as the total recovered strain or force. As a result, simplified phenomenological models have been increasingly adopted to capture the kinetics of shape-memory activation under thermal stimuli, especially when full constitutive descriptions are not required for

system-level design [31]. In this context, sigmoidal and logistic-type functions have proven effective in representing recovery evolution over time, as they naturally describe the gradual onset, rapid transition, and saturation stages typically observed in SMP recovery processes [32]. In particular, logistic functions provide a compact mathematical description of recovery behavior using a limited number of physically interpretable parameters, such as characteristic recovery time, maximum recovered strain or force, and recovery rate. Such functions have been successfully applied to model strain recovery, displacement evolution, and thermally driven transformation kinetics in polymeric and SMP-based systems, demonstrating good agreement with experimental observations while maintaining computational simplicity [32,33]. Fig. 1 illustrates the general form of a logistic (sigmoid) function [34], highlighting its suitability for modeling the time-dependent recovery response of SMPs.

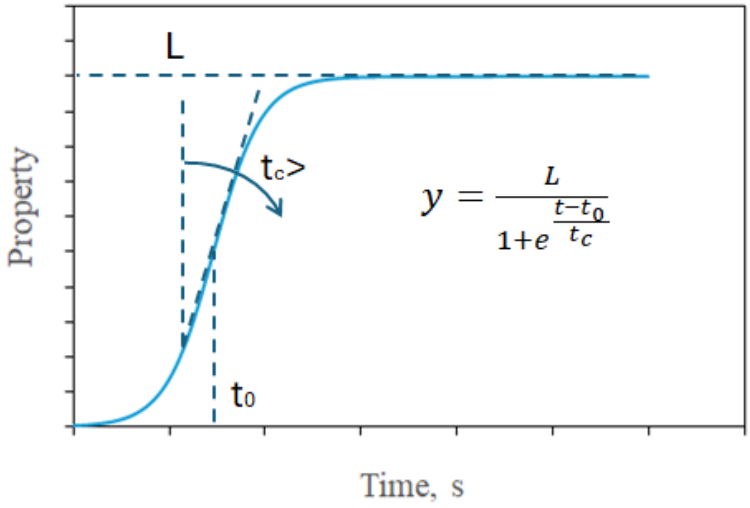

Fig. 1. Logistic function, also known as the sigmoid function, over time

Despite these advances in experimental characterization and modeling, the thermomechanical response of FDM-printed TPU-based SMPs under constrained recovery conditions remains insufficiently explored. While many studies have focused on free recovery behavior, significantly fewer have investigated the recovery forces generated when shape restoration is mechanically constrained. Recovery force is a critical parameter for the design of soft actuators, deployable structures, and biomedical devices that must perform mechanical work or sustain external loads during activation. Furthermore, existing investigations predominantly focus on general-purpose TPUs, whereas biomedical-grade TPUs—despite their relevance for medical and assistive technologies—remain largely unexplored in terms of constrained shape-memory actuation.

The present study addresses these gaps by investigating the recovery forces of FDM-printed biomedical-grade TPU specimens under constrained recovery conditions. Block-shaped samples with controlled geometry were fabricated via fused deposition modeling, mechanically programmed into a temporary C-shaped configuration, fixed at subzero temperature, and subsequently activated at room temperature under mechanical constraint. The evolution of recovery load over time was experimentally measured and modeled using a logistic function to identify characteristic recovery parameters.

Materials and Methods

Modelling. The transition of such properties of organic materials as a function of time is often represented by a sigmoidal curve, as the logistic function of Fig. 1, which is the analytical solution of the Verhulst logistic differential equation [34], commonly written:

$$y = \frac{L}{1+e^{-k(x-x_0)}} = \frac{L}{1+e^{\frac{t-t_0}{t_c}}} \quad (1)$$

where the term L is the value of the long-time plateau, t_0 (or x_0) is the curve inflection point and represents the time at which the rate of the property change reaches its maximum, and k (or $-1/t_c$) represents the growth-rate parameter. In this case, t_c is a characteristic time which influences the slope of the linear trend. This simple law has all the necessary parameters for the characterization of material behavior.

Materials. The material used in this study is a commercially available thermoplastic polyurethane (TPU), chosen to ensure reproducibility, standardization, and quality control, facilitating reliable and widely comparable results. The material was used as received, without any purification or modification. Commercial TPU pellets (DiAPLEX MM3510) were purchased from SMP Technologies Inc. (Tokyo, Japan). According to the manufacturer, the material properties are the following: glass transition temperature (Tg) of 35 °C, tensile strength of 51 MPa, bending strength and modulus of 85 MPa and 2450 MPa, respectively, and a density of 1.25 g/cm^3. This TPU is designed for biomedical applications and was selected for its potential in soft actuators intended for contact with the human body, as its Tg near body temperature enhances its use for such applications.

Table 1. FDM parameters used in TPU printing

	A	B	C	D
Nozzle temperature [°C]	240	240	240	240
Nozzle diameter [mm]	0.4	0.4	0.2	0.8
Printer bed temperature [°C]	50	50	50	50
Printing speed [mm/s]	40	40	40	40
Infill	100%	100%	100%	100%
Pattern	linear	linear	linear	linear
Raster angle	45°	45°	45°	45°
Layer thickness [mm]	0.2	0.3	0.15	0.3
Retraction length [mm]	0.8	0.8	0.8	0.8

Table 2. Properties of the printed samples

Sample	Thickness, mm	Masst, g	Apparent density, g/cm^3	Bending load, N
A	4.00	5.79	0.80	3.2
B	5.18	8.64	0.93	11.9
C	3.83	6.82	0.99	9.8
D	4.31	8.69	1.12	11.5

3D Printing Filament Production. The TPU filament was produced using a 3DEVO Composer 450 filament extruder. The machine features a 2 L hopper for pellet loading, four independently controlled heating zones (maximum temperature 450 °C), and a single-screw extruder with a speed range of 2–15 rpm. A spooling system adjusts the winding speed based on real-time filament diameter measurements, and two cooling fans are installed at the nozzle exit to ensure dimensional stability. Multiple trial runs were conducted to optimize the extrusion parameters, ranging the heating zone temperatures from 160° to 200°C, the extruder speed from 3.5 to 4.0 rpm, and the fan speed from 60% to 100%. The processing window for filament extrusion was determined using the operating parameters recommended by the machine manufacturer for commercial TPU. The final optimized conditions were as follows: heating zone temperatures of 170 °C, 190 °C, 195 °C, and 193 °C from the hopper to the nozzle, respectively; an extruder speed of 3.7 rpm; and a fan speed of 80%. The resulting filament had a diameter of 1.75 ± 0.1 mm. After extrusion, the polymer was automatically collected and wound onto a spool for subsequent 3D printing.

Sample Fabrication. Rectangular samples were designed for thermo-mechanical shape-memory testing, with final dimensions of 30 × 60 mm^2. The samples were printed using a commercial Fused Deposition Modeling (FDM) printer (Prusa i3 MK3S+, Prusa Research, Czech Republic). Key parameters were adjusted during a first optimization study included nozzle temperature (210–240 °C) and printing speed (20–40 mm/s) [35]. In this study, four different combinations of nozzle diameter and layer thicknesses were selected as printing parameters as reported in Table 1. Some physical properties of the four different printed samples are reported in Table 2.

Recovery Force and Time Measurement. The printed TPU samples were deformed and clamped in a fixed configuration. This configuration was a curved shape with a radius of 10 mm, as reported in Fig. 2, where a deformed sample is shown together with its temperature map at the beginning of the test. The load to achieve the final sample deformation at room temperature is reported in Table 1 as bending load. In the constrained recovery test, after deformation, the samples were stored in a fridge at –22 °C to maintain the temporary shape. Recovery was initiated by transferring the samples to ambient temperature, allowing the thermally triggered shape-memory effect to occur naturally. An infrared (IR) camera (Testo 883, by Testo S.p.A., Settimo Milanese (MI), Italy) was used to monitor the sample surface temperature throughout recovery, while a universal testing machine (Insight 5, MTS System Corp.), recorded the corresponding recovery force and the time required for the sample to return toward its original configuration.

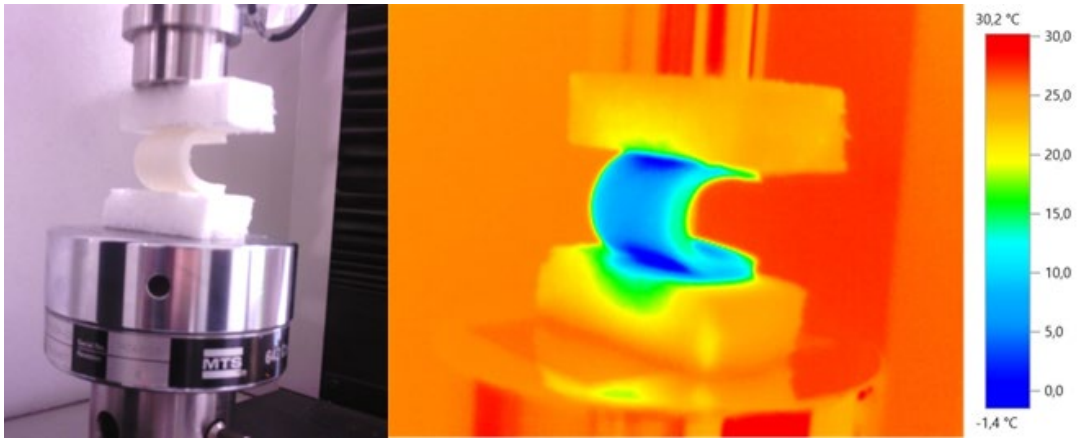

Fig. 2. Constrained recovery test of a 3D-printed sample and thermal image at the beginning and the end of the test

Specifically, the memorized sample was positioned between two compression plates, and the force exerted on the load cell (nominal maximum load 100 N, MTS Systems Corp.) during recovery phase was recorded. Small PET foam blocks were inserted to prevent direct contact with the metallic platens, while temperature evolution during recovery was monitored with a thermal camera (as shown in Fig. 2). The recovery loads and times were acquired during tests. This setup enabled precise measurement of recovery force evolution and timing under passive thermal activation conditions.

Results and Discussion

Results of the constrained recovery tests are reported in Fig. 3 for the 4 different printed samples. In all these cases, the load increase depends on the sample heating in room conditions, after taking the sample from the fridge. A partial recovery is expected as a result of the time required to position the sample between the platens and initiate the test, which is longer for thinner or denser specimens. Nevertheless, infrared thermography indicates that the initial conditions were highly consistent across all samples, with a minimum surface temperature below 0 °C. By considering the maximum load of the curves of Fig. 3, it reaches 3.8 N for sample A, 13.3 N for sample B, 8.7 N for sample C and 10.5 N for sample D. Apparently, there is no direct correlation between these load values and the sample

thickness or density, even if they approach the bending load of Table 2. The reason is that the sample thickness and void fraction influence both the sample stiffness.

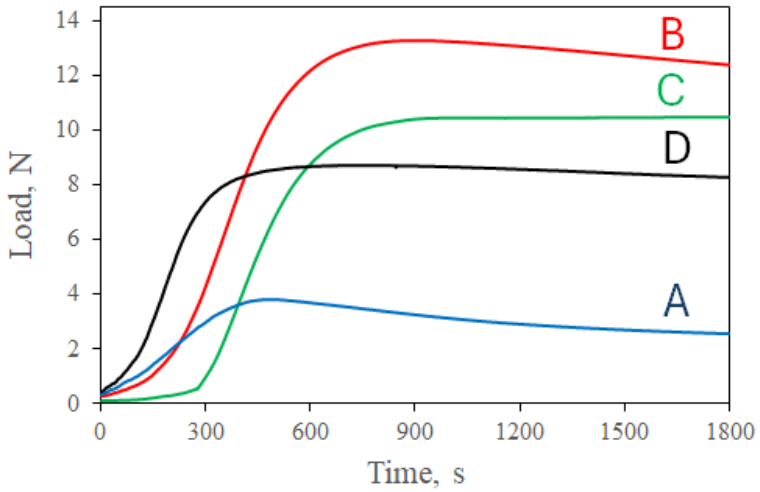

Fig. 3. Load curves from constrained recovery test of the 3D-printed samples

As a first approximation, the simple bent-beam model assumes that the bending stiffness of the beam is proportional to the term $v_f T^3$, where v_f is the volume fraction of the porous material with a given bulk elastic modulus (in this case, the biomedical polyurethane), and T is the sample thickness. This parameter can be calculated from the data reported in Table 2 and the bulk resin density. As shown in Fig. 4a, both the maximum load measured during the constrained recovery test (Fig. 3) and the bending load at room temperature (Table 2) exhibit a strong correlation with this parameter, indicating their dependence on sample stiffness. However, the correlation is not linear, as might be expected, and a plateau is observed at high volume fractions. This behavior suggests that nonlinear effects and possible material plasticization occur during the memory stage, enabling the material to reach the final C-shaped configuration shown in Fig. 2.

The constrained recovery curves show a quasi-sigmoidal behavior, as a small peak is reached before the plateau. This maximum is very small in curve D, and absent in curve C but evident in curves A and B. It depends on the fact that the maximum recovery load is not obtained at room temperature but an intermediate temperature between the beginning and the end of the heating phase. The occurrence and the intensity of this maximum load is strongly influenced by the heating rate of the samples, disappearing at very low rates. As the heating phase was not controlled during the test, its occurrence is not well replicated in all the samples.

The model of equation (1) has been applied after curve normalization. The values of each curve have been divided by the maximum of the same curve, which is very close to the final plateau, apart from curve A. By this normalization, the term L of equation (1) is equal to 1 for all the curves. Moreover, the curves of samples A, B and D have been shifted along the time axis to be superimposed on the curve of sample C. This shift is equal to 270 s for sample A, 80 s for sample B, and 250 s for sample C. Fig. 4b shows that curves are well superimposed after this shift operation, and are optimally fitted by equation (1) with a t_0 of 440 s, and a t_c of 75 s.

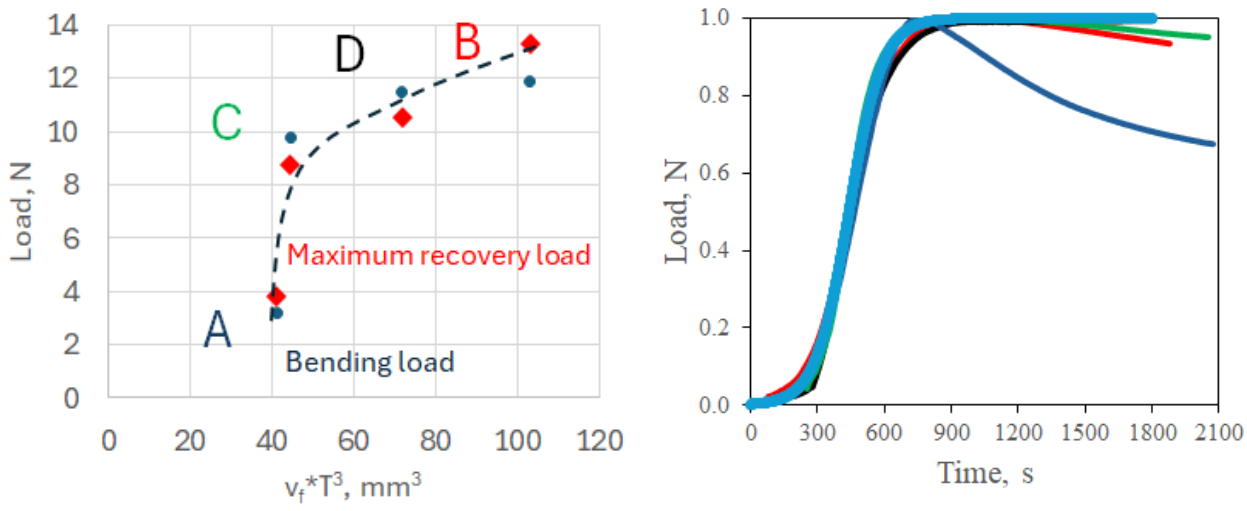

a) b)

Fig. 4. Load data of the different 3D-printed samples (a) and optimal fitting of the experimental load curves by the proposed sigmoidal function (b)

Differences in the inflection point t_0 are related to the different transition onset, which is not directly modeled in equation (1) and is influenced by the heating conditions. A trend in t_0 is not observed because of the different room conditions during the transition and the bulk thermal diffusivity of the samples. Nevertheless, all the curves show the same characteristic time t_c, which is related to the intrinsic time for the event occurrence. A time of 75 s means that the process can be observed at naked eye but slowly. As all the 3D-printed samples show the same t_0, despite the different conditions during transition, the term t_c becomes representative of the nature of the printed polymer and is independent of the printing conditions.

Experimentally, not all the curves show a plateau at long times, and generally a maximum is expected after the linear trend. In fact, the maximum originates because the exerted load at low temperature is higher than the load at room temperature, being the polymer stiffer. With temperature increase, the polymer mobility improves, therefore its softness and its speed of actuation. Therefore, this aspect is related to the heating conditions during transition, as well as the onset time, but it does not affect the shape of the transition region too. The term t_c can be used to characterize the polymer shape memory, apart from its printing conditions.

Summary

Biomedical devices can be fabricated by 3D printing using biocompatible polyurethanes, with shape recovery or actuation functionalities incorporated when required. This study demonstrates that the shape-memory behavior of 3D-printed porous samples follows a common sigmoidal law, regardless of the printing conditions, indicating an intrinsic material response. Constrained recovery tests revealed that the actuation load is governed by the effective bending stiffness of the samples, which can be tailored through the printing strategy by controlling thickness and volume fraction. Although a strong correlation with stiffness was observed, nonlinear effects and material plasticization lead to a saturation of the recovery load at high volume fractions. After normalization and time alignment, all recovery curves collapsed onto a single master curve characterized by a common intrinsic time constant. Actuation loads exceeding 12 N were achieved experimentally, highlighting the potential for designing mechanically programmable, shape-memory biomedical devices.

Acknowledgments

This paper and the research behind it would not have been possible without the exceptional support of our laboratory technician, Fabrizio Betti. This study was carried out within the "4D Printing of smart soft robotics (4D P.Ro.)" and received funding from the Research Projects of Significant National Interest (PRIN) 2022 PNRR, project n. 2022SFF349, with CUP Master D53D23004020008.

References

[1] R. Zende, V. Ghase, V. Jamdar, A review on shape memory polymers, Polym. Technol. Mater. 62 (2023) 467–485.

[2] Y. Zhu, J. Hu, Y. Liu, Shape memory effect of thermoplastic segmented polyurethanes with self-complementary quadruple hydrogen bonding in soft segments, Eur. Phys. J. E 28 (2009) 3-10.

[3] F. Ji, J. Li, Y. Weng, J. Ren, Synthesis of PLA-based thermoplastic elastomer and study on preparation and properties of PLA-based shape memory polymers, Mater. Res. Express 7 (2020) 015315.

[4] M. R. Pfau, K. G. McKinzey, A. A. Roth, M. A. Grunlan, PCL-based shape memory polymer semi-IPNs: the role of miscibility in tuning the degradation rate, Biomacromolecules 21 (2020) 2493–2501.

[5] K. Kojio, M. Furukawa, Y. Nonaka, S. Nakamura, Control of mechanical properties of thermoplastic polyurethane elastomers by restriction of crystallization of soft segment, Materials 3(2010) 5097–5110.

[6] A. Boubakri, N. Haddar, K. Elleuch, Y. Bienvenu, Impact of aging conditions on mechanical properties of thermoplastic polyurethane, Mater. Des. 31 (2010) 4194–4201.

[7] J. Datta, P. Kasprzyk, Thermoplastic polyurethanes derived from petrochemical or renewable resources: A comprehensive review, Polym. Eng. Sci. 58 (2018) E14 - E35.

[8] A. Mishra, K. Seethamraju, J. Delaney, P. Willoughby, R. Faust, Long-term in vitro hydrolytic stability of thermoplastic polyurethanes, J. Biomed. Mater. Res. Part A 103 (2015) 3798–3806.

[9] D. Cozzens, U. Ojha, P. Kulkarni, R. Faust, S. Desai, Long term in vitro biostability of segmented polyisobutylene-based thermoplastic polyurethanes, J. Biomed. Mater. Res. Part A 95A (2010), 774–782.

[10] H.-Y. Mi, X. Jing, B. N. Napiwocki, B. S. Hagerty, G. Chen, L.-S. Turng, Biocompatible, degradable thermoplastic polyurethane based on polycaprolactone-block-polytetrahydrofuran-block-polycaprolactone copolymers for soft tissue engineering, J. Mater. Chem. B 5 (2017) 4137–4151.

[11] R. Al Nakib, A. Toncheva, V. Fontaine, J. Vanheuverzwijn, J. Raquez, F. Meyer, Thermoplastic polyurethanes for bi-omedical application: A synthetic, mechanical, antibacterial, and cytotoxic study, J. Appl. Polym. Sci. 139 (2022), .

[12] M.-S. M'Bengue, T. Mesnard, F. Chai, M. Maton, V. Gaucher, N. Tabary, M.-J. García-Fernandez, J. Sobocinski, B. Martel, N. Blanchemain, Evaluation of a medical grade thermoplastic polyurethane for the manufacture of an implantable medical device: the impact of FDM 3D-printing and gamma sterilization, Pharmaceutics 15 (2023) 456.

[13] S. Kumar, R. Singh, A.P. Singh, Y. Wei, Three-dimensional printed thermoplastic polyurethane on fabric as wearable smart sensors, Proc. Inst. Mech. Eng. Part L J. Mater. Des. Appl. 237 (2023) 1678–1692

[14] S. Lepak-Kuc, B. Podsiadły, A. Skalski, D. Janczak, M. Jakubowska, A. Lekawa-Raus, Highly Conductive carbon nanotube-thermoplastic polyurethane nanocomposite for smart clothing applications and beyond, Nanomaterials 9 (2019) 1287.

[15] P. Awasthi, S. S. Banerjee, Construction of stimuli-responsive and mechanically-adaptive thermoplastic elastomeric materials, Polymer (Guildf). 259 (2022) 125338.

[16] Y. Zan, M. Piedrahita-Bello, S. E. Alavi, G. Molnár, B. Tondu, L. Salmon, A. Bousseksou, Soft actuators based on spin-crossover particles embedded in thermoplastic polyurethane, Adv. Intell. Syst. 5 (2023).

[17] C. Li, H. Xia, J. Yao, Q.-Q. Ni, Electrically induced soft actuators based on thermoplastic polyurethane and their actuation performances including tiny force measurement, Polymer (Guildf). 180 (2019) 121678.

[18] O. Yasa, Y. Toshimitsu, M.Y. Michelis, L. Jones, M. Filippi, T. Buchner, R.K. Katzschmann, An overview of soft robotics, Annu. Rev. Control. Robot. Auton. Syst. 6 (2023) 1–29

[19] C. Lee, M. Kim, Y.J. Kim, N. Hong, S. Ryu, H.J. Kim, S. Kim, Soft robot review. Int. J. Control. Autom. Syst. 2017, 15, 3–15

[20] F.B. Koehler, T.M. Sanderson, D.L. Safranski, K. Gall, V. Jaker, J. Orrock, C. Holshauser, 3D printing of thermoplastic polyurethane shape memory polymer, In CamX: Composites and Advanced Materials Expo (2015) 2231–2245

[21] L. Ritzen, V. Montano, S.J. Garcia, 3D printing of a self-healing thermoplastic polyurethane through FDM: from polymer slab to mechanical assessment, Polymers, 13(2) (2021) 305.

[22] D. Rigotti, A. Dorigato, A. Pegoretti, 3D printable thermoplastic polyurethane blends with thermal energy storage/release capabilities, Mater. Today Commun 17 (2018). 54–60.

[23] D.B. Rahmatabadi, L. Brasileiro Quirino Brito, R. B. Cunha, P. Agrawal, G. de Figueiredo Brito, 4D printing of shape memory polyethylene terephthalate glycol/thermoplastic polyurethane (PETG/TPU) blends, J. Manuf. Process. 119 (2024) 596-608.

[24] B. Peng, X. Wang, M. Zhang, Fused Filament Fabrication 4D Printing of a Highly Extensible, Shape-Memory and Self-Healing Polymer Blend, ACS Appl. Mater. Interfaces. 12(42), (2020) 47018–47027.

[25] I. Jung, K. Jung, Shape recovery properties of 3D printed re-entrant strip using shape memory thermoplastic polyurethane (SMTPU), Fash. Text. 10 (2023), 48.

[26] E.M. Arruda, M.C. Boyce, R. Jayachandran, Effects of strain rate, temperature and thermomechanical coupling on the finite strain deformation of glassy polymers, Mech. Mater, 19 (1995) 193–212.

[27] Y. Liu, K. Gall, M. L. Dunn, A. R. Greenberg, J. Diani, Thermomechanics of shape memory polymers: uniaxial experiments and constitutive modeling, Int. J. Plast22, (2006) 279–313.

[28] J. Diani, B. Fayolle, P. Gilormini, A review on the thermomechanical behaviour of shape memory polymers, Eur. Polym. J48 (2012) 1387–1402.

[29] T.D. Nguyen, H.J. Qi, F. Castro, K.N. Long, A thermoviscoelastic model for amorphous shape memory polymers: Incorporating structural and stress relaxation, Mech. Phys. Solids 56 (2008) 2792–2814.

[30] Y. Chen, D. C. Lagoudas, A constitutive theory for shape memory polymers. Part I: Large deformation thermomechanics, Mech. Phys. Solids 56 (2008) 1752–1765.

[31] H.J. Qi, T.D. Nguyen, F. Castro, C.M. Yakacki, R. Shandas, Finite deformation thermomechanical behavior of thermally induced shape memory polymers, Mech. Phys. Solids 56, (2008) 1730–1751.

[32] C. M. Yakacki, R. Shandas, D. Safranski, A. M. Ortega, K. Sassaman, K. Gall, Strong, tailored, biocompatible shape-memory polymer networks, Adv. Funct. Mater 18(2008) 2428–2435.

[33] E. Ghobadi, M. Elsayed, R. Krause-Rehberg, H. Steeb, Demonstrating the influence of physical aging on the functional properties of shape-memory polymers, Polymers 10(2) (2018)107.

[34] E.W. Weisstein, Logistic equation. In MathWorld—A Wolfram Web Resource. Retrieved February 11, 2026, from https://mathworld.wolfram.com/LogisticEquation.html

[35] L. Burratti, D. Bellisario, F. Quadrini, L. Iorio, L. Santo, 3D printing of soft actuators in nano-filled shape memory thermoplastic polyurethane, Mater. Res. Proc 54 (2025) 2047.